Slow photoelectron imaging spectroscopy of CCO^- and CCS^-

Etienne Garand,[1] Tara I. Yacovitch,[1] and Daniel M. Neumark[1,2,a)]
[1]*Department of Chemistry, University of California Berkeley, Berkeley, California 94720, USA*
[2]*Chemical Sciences Division, Lawrence Berkeley National Laboratory, Berkeley, California, 94720, USA*

(Received 17 June 2008; accepted 21 July 2008; published online 20 August 2008)

High-resolution photodetachment spectra of CCO^- and CCS^- using slow photoelectron velocity-map imaging spectroscopy are reported. Well-resolved transitions to the neutral $X\ ^3\Sigma^-$, $a\ ^1\Delta$, $b\ ^1\Sigma^+$, and $A\ ^3\Pi$ states are seen for both species. The electron affinities of CCO and CCS are determined to be 2.3107 ± 0.0006 and 2.7475 ± 0.0006 eV, respectively, and precise term energies for the $a\ ^1\Delta$, $b\ ^1\Sigma^+$, and $A\ ^3\Pi$ excited states are also determined. The two low-lying singlet states of CCS are observed for the first time, as are several vibronic transitions within the four bands. Analysis of hot bands finds the spin-orbit orbit splitting in the $X\ ^2\Pi$ ground state of CCO^- and CCS^- to be 61 and 195 cm^{-1}, respectively. © *2008 American Institute of Physics*.
[DOI: 10.1063/1.2969819]

I. INTRODUCTION

The isovalent CCO and CCS radicals are important constituents of the interstellar medium.[1,2] The CCO radical is a key intermediate in hydrocarbon combustion.[3–5] CCS microwave absorption is used as a molecular probe of the velocity, density, and age of dark interstellar clouds[6,7] These species also serve as case studies for the theoretical treatment of spin-rovibronic interaction and vibronic coupling in linear triatomic molecules with triplet states.[8,9] The CCO and CCS radicals are known to have several low-lying singlet and triplet electronic states. While the $X\ ^3\Sigma^-$ ground state and the first optically accessible electronic state ($A\ ^3\Pi$) of these species have been studied in detail both experimentally and theoretically, less information is available on the singlet states. In this paper, high-resolution photodetachment spectra of the CCO^- and CCS^- anions are reported, which provide a detailed probe of the low-lying triplet and singlet states of both neutral radicals.

The CCO radical has been studied by microwave spectroscopy,[10,11] infrared and UV absorption spectroscopy,[12–22] and laser-induced fluorescence (LIF).[23] Similarly, CCS has been investigated with microwave spectroscopy,[2,24,25] infrared and UV absorption spectroscopy,[26–28] and LIF.[29,30] These experiments have provided the rotational constants and some vibrational frequencies of the $X\ ^3\Sigma^-$ and $A\ ^3\Pi$ electronic states. Accordingly, most of the theoretical work on the CCO and CCS radicals has also focused on the structure of these two states as well as the Renner–Teller coupling in the upper state.[8,9,29,31–35] Some calculations on the energetic and structures of the other low-lying electronic states have also been reported.[27,36–38]

The corresponding CCO^- and CCS^- anions have been the subject of a few experimental and theoretical investigations. Maier and co-workers have observed the $X\ ^2\Pi \leftarrow A\ ^2\Sigma^+$ absorption of both ions in a neon matrix.[27,39] Electronic structure calculations of these two states have been reported[27,37] as well as a theoretical investigation of the Renner–Teller effect in the ground state.[40,41]

Additional information on the CCO^- anion and CCO neutral is obtained from the anion photoelectron (PE) spectrum.[37,42,43] The PE spectrum yielded an electron affinity of 2.310 ± 0.012 eV (Ref. 42) and provided the first experimental observation of the neutral singlet states. The anion has a $\cdots(6\sigma)^2(1\pi)^4(7\sigma)^2(2\pi)^3$ molecular orbital configuration. The removal of a 2π electron leads to the $X\ ^3\Sigma^-$, $a\ ^1\Delta$, and $b\ ^1\Sigma^+$ neutral states, while the removal of a 7σ electron produces the $A\ ^3\Pi$ state. Hence, PE spectroscopy probes all four low-lying neutral states on equal footing, providing not only electronic state energies but also the vibrational frequencies for the Franck–Condon (FC) active vibrational modes in both the ground and excited states. In addition, the observation of nominally forbidden vibrational excitations provides information on vibronic coupling interactions among these states.

In this paper, we report the high-resolution photodetachment spectra of CCO^- and CCS^- using slow photoelectron velocity-map imaging (SEVI) spectroscopy. The SEVI spectra for CCO^- have considerably higher resolution than the previous PE spectra. This work also represents the first photodetachment experiment on CCS^- and the first observation of the low-lying singlet states of CCS. It provides precise electron affinities for CCO and CCS, as well as term energies for the neutral $a\ ^1\Delta$, $b\ ^1\Sigma^+$, and $A\ ^3\Pi$ electronic states of both species. The positions of several previously unobserved vibronic transitions within the four electronic bands are reported and assigned.

II. EXPERIMENTAL

The SEVI apparatus has been described in detail elsewhere.[44,45] In SEVI, a high-resolution variant of PE spectroscopy, mass-selected anions are photodetached at a series of wavelengths. The resulting photoelectrons are collected by

a)Author to whom correspondence should be addressed. Electronic mail: dneumark@berkeley.edu.

 © 2008 American Institute of Physics

Downloaded 21 Aug 2008 to 169.229.32.135. Redistribution subject to AIP license or copyright; see http://jcp.aip.org/jcp/copyright.jsp

velocity-map imaging[46] (VMI) using relatively low extraction voltages, with the goal of selectively detecting slow electrons with high efficiency and enlarging their image on the detector. At each wavelength, one obtains a high-resolution photoelectron spectrum over a limited range of electron kinetic energy.

CCO^- anions were produced from a gas mixture comprising 1% acetylene, 8% O_2, and 20% CO_2 in a balance of Ar. Similarly, CCS^- anions were produced from 1% acetylene, 1% CS_2, and 30% CO_2 in a balance of argon. The gas mixture, at a stagnation pressure of 300 psi, was expanded into the source vacuum chamber through an Even–Lavie pulsed valve[47] equipped with a circular ionizer. Anions formed in the gas expansion were perpendicularly extracted into a Wiley–McLaren time-of-flight mass spectrometer[48] and directed to the detachment region by a series of electrostatic lenses and pinholes. A pulse on the last ion deflector allowed only the desired mass into the interaction region. Anions were photodetached between the repeller and the extraction plates of the VMI stack by the focused output of a Nd:YAG (yttrium aluminum garnet) pumped tunable dye laser. The PE cloud formed was then coaxially extracted down a 50 cm flight tube and mapped onto a detector comprising a chevron-mounted pair of time-gated imaging quality microchannel plates coupled to a phosphor screen, as is typically used in photofragment imaging experiments.[49] Events on the screen were collected by a 1024×1024 charge-coupled device camera and sent to a computer. Electron velocity-mapped images resulting from 30 000–50 000 laser pulses were summed, quadrant symmetrized, and inverse-Abel transformed. PE spectra were obtained via angular integration of the transformed images.

The apparatus was calibrated by acquiring SEVI images of atomic chloride and sulfur at several different photon energies. With the 350 V VMI repeller voltage used in this study, the full widths at half maximum of the chloride peaks were 3.3 cm^{-1} at 24 cm^{-1} above threshold. In the SEVI experiment, within the same image, all observed transitions have similar widths in pixels (Δr), which means transitions observed further from threshold (larger r) are broader in energy. By varying the laser wavelength, a series of images in which the transitions of interest are close to the detachment threshold can be acquired, yielding high resolution through the entire PE spectra. The PE spectra presented here are plotted with respect to electron binding energy (eBE), defined as the difference between the energy of the photodetachment photon and the measured electron kinetic energy.

SEVI also provides information on the photoelectron angular distribution (PAD). For one-photon detachment, the PAD is given by[50]

$$\frac{d\sigma}{d\Omega} = \frac{\sigma_{\text{total}}}{4\pi}\left(1 + \beta\left(\frac{3}{2}\cos^2(\theta) - \frac{1}{2}\right)\right), \quad (1)$$

where θ is the angle between the direction of the PE ejection and the polarization vector of the incident photon. The anisotropy parameter β lies between 2 and −1 and provides information on the orbital angular momentum (l) of the ejected PE; $l=0$ (s-wave) detachment leads to $\beta=0$, $l=1$ (p-wave) to $\beta=2$, and $l=0$ and 2 in equal amplitude ($s+d$ wave) to $\beta=-1$. Generally, the value of β depends on the detachment energy[44] and thus peaks having $\beta>1$ are simply labeled as "p" while those with $\beta<0.2$ or negative are labeled as "$s+d$."

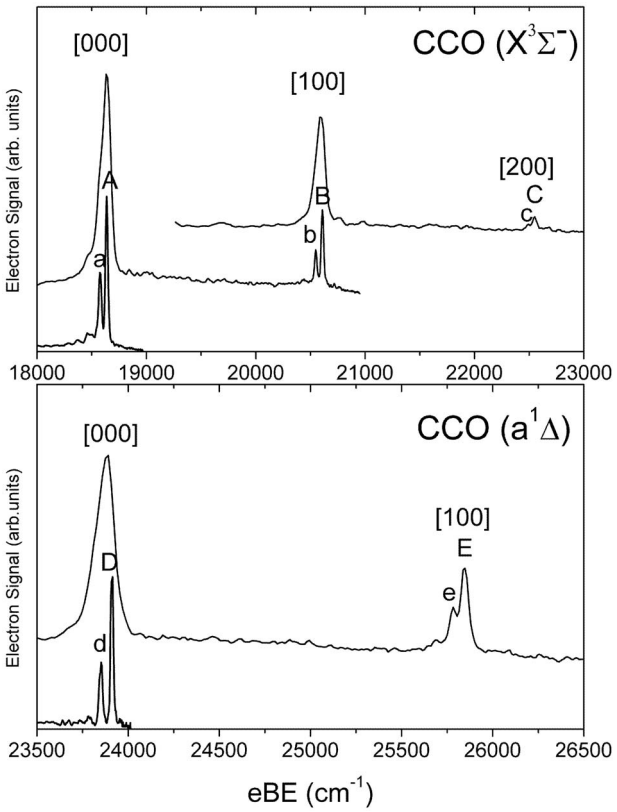

FIG. 1. SEVI spectra of CCO^- in the 18 000–26 500 cm^{-1} eBE range. The top panel displays traces taken at photon energies of 24 242, 21 097, and 19 084 cm^{-1}, while the lower panel displays traces taken at 27 322 and 24 242 cm^{-1}. The traces are vertically offset for clarity.

III. RESULTS AND ASSIGNMENTS

A. CCO^-

SEVI spectra of CCO^- covering the eBE range from 18 000 to 33 500 cm^{-1} are shown in Figs. 1 and 2. The spectra comprise seven SEVI traces taken at different photon energies. The peak positions, PAD, and assignments are summarized in Table I. Our spectra are similar to the previously reported PE spectra[37,42] but with much higher resolution.

The SEVI spectra are divided into four bands of peaks, each corresponding to transitions to a different neutral electronic state. Peaks A, D, F, and I are assigned to the vibronic origins of the $X\ ^3\Sigma^-$, $a\ ^1\Delta$, $b\ ^1\Sigma^+$, and $A\ ^3\Pi$ states, respectively, based on the calculation of Zengin *et al.*[37] and the previous PE spectra.[37,42] These assignments are supported by the PADs. All the features at eBE below that of peak I have an $s+d$ PAD, which is consistent with detachment from the 2π orbital leading to the $X\ ^3\Sigma^-$, $a\ ^1\Delta$, and $b\ ^1\Sigma^+$ states. The PADs for peak I and those at higher eBE have p-wave character, consistent with detachment from the 7σ orbital producing the $A\ ^3\Pi$ state.

The CCO^- SEVI spectra are dominated by the vibrational origin transitions. In the top panel of Fig. 1, peaks B

Downloaded 21 Aug 2008 to 169.229.32.135. Redistribution subject to AIP license or copyright; see http://jcp.aip.org/jcp/copyright.jsp

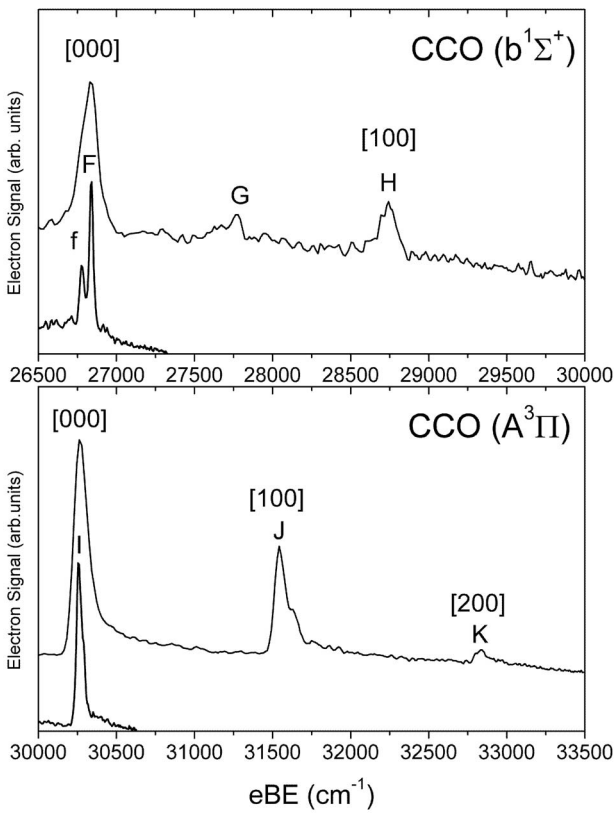

FIG. 2. SEVI spectra of CCO^- in the 26 500–33 500 cm^{-1} eBE range. The top panel displays traces taken at photon energies of 30 628 and 27 322 cm^{-1}, while the lower panel displays traces taken at 33 557 and 30 628 cm^{-1}. The traces are vertically offset for clarity.

and C are assigned to the 1_0^1 and 1_0^2 photodetachment transitions within the $X\ ^3\Sigma^-$ band. This assignment yields a value of 1973 cm^{-1} for the ν_1 fundamental, in excellent agreement with the value of 1971 cm^{-1} found in the infrared diode laser measurement of Moazzen-Ahmadi *et al.*[20] Peaks E and G are assigned to the same 1_0^1 and 1_0^2 transitions within the $a\ ^1\Delta$ band, while peak H is assigned to the 1_0^1 transition of the $b\ ^1\Sigma^+$ state. These assignments yield fundamental ν_1 frequencies of 1934 and 1900 cm^{-1} for the $a\ ^1\Delta$ and $b\ ^1\Sigma^+$ singlet states, respectively. The only other experimental observations of these modes come from the lower resolution PE spectra.[37,42] In Fig. 1 and in the top panel of Fig. 2, peaks a–f are found to lie systematically 61 cm^{-1} below a major transition. These peaks are assigned to transitions originating from the excited spin-orbit state ($X\ ^2\Pi_{1/2}$) of the anion. This assignment agrees with the calculations by Panten *et al.*,[40] which predicted a spin-orbit splitting of −57.5 cm^{-1} for CCO^-. Finally, in the lower panel of Fig. 2, peaks J and K are assigned to the 3_0^1 and 3_0^2 transitions within the $A\ ^3\Pi$ band. This state is subject to spin-orbit splitting on the order of 36 cm^{-1}.[8,17] However, the *p*-wave nature of peaks I, J, and K prevent the observation of the individual spin-orbit levels since the photodetachment cross section is too small at wavelengths sufficiently close to threshold to resolve them.[51,52]

B. CCS^-

SEVI spectra of CCS^- covering the eBE range from 21 800 to 33 500 cm^{-1} are shown in Figs. 3 and 4. The spectra comprise seven SEVI traces taken at different photon energies. Peak positions, PADs, and assignments for the CCS^- SEVI spectra are summarized in Table II. These are the first PE spectra of CCS^- reported. Peaks A, J, Q, and U are the main spectral features and are assigned to the vibronic origins of the $X\ ^3\Sigma^-$, $a\ ^1\Delta$, $b\ ^1\Sigma^+$, and $A\ ^3\Pi$ states, respectively, by analogy to the CCO^- spectra. This assignment is also consistent with the calculated term energies of these states.[27,38] Just as in the CCO^- spectra, all the features at eBE below the $A\ ^3\Pi$ origin (peak U), with the exception of

TABLE I. Peak Positions, PAD, and assignments for the CCO^- SEVI spectra.

Peak	Position (cm^{-1})	Offset (cm^{-1})	PAD	Previous Obs. (cm^{-1})	Calculated (cm^{-1})	Assignment (Vib)	Assignment (Electronic states)
a	18 576	−61	*s+d*			0_0^0	$X\ ^3\Sigma^- \leftarrow X\ ^2\Pi_{1/2}$
A	18 637	0	*s+d*			0_0^0	$X\ ^3\Sigma^- \leftarrow X\ ^2\Pi_{3/2}$
b	20 549	1912	*s+d*			1_0^1	$X\ ^3\Sigma^- \leftarrow X\ ^2\Pi_{1/2}$
B	20 610	1973	*s+d*	1971[a], 1960[b]	1949[c]	1_0^1	$X\ ^3\Sigma^- \leftarrow X\ ^2\Pi_{3/2}$
c	22 489	3852	*s+d*			1_0^2	$X\ ^3\Sigma^- \leftarrow X\ ^2\Pi_{1/2}$
C	22 550	3913	*s+d*	3976[b]		1_0^2	$X\ ^3\Sigma^- \leftarrow X\ ^2\Pi_{3/2}$
d	23 850	−61	*s+d*			0_0^0	$a\ ^1\Delta \leftarrow X\ ^2\Pi_{1/2}$
D	23 911	0	*s+d*			0_0^0	$a\ ^1\Delta \leftarrow X\ ^2\Pi_{3/2}$
e	25 784	1873	*s+d*			1_0^1	$a\ ^1\Delta \leftarrow X\ ^2\Pi_{1/2}$
E	25 845	1934	*s+d*	1943[d], 1944[b]	2005[e]	1_0^1	$a\ ^1\Delta \leftarrow X\ ^2\Pi_{3/2}$
f	26 779	−61	*s+d*			0_0^0	$b\ ^1\Sigma^+ \leftarrow X\ ^2\Pi_{1/2}$
F	26 840	0	*s+d*			0_0^0	$b\ ^1\Sigma^+ \leftarrow X\ ^2\Pi_{3/2}$
G	27 762	3851	*s+d*			1_0^2	$a\ ^1\Delta \leftarrow X\ ^2\Pi_{3/2}$
H	28 740	1900	*s+d*	1823[b]	2022[e]	1_0^1	$b\ ^1\Sigma^+ \leftarrow X\ ^2\Pi_{3/2}$
I	30 258	0	*p*	1282[f]		0_0^0	$A\ ^3\Pi_2 \leftarrow X\ ^2\Pi_{3/2}$
J	31 537	1279	*p*	1266[b]	1271[c]	3_0^1	$A\ ^3\Pi_2 \leftarrow X\ ^2\Pi_{3/2}$
K	32 831	2573	*p*	2565[b]		3_0^2	$A\ ^3\Pi_2 \leftarrow X\ ^2\Pi_{3/2}$

[a]Reference 20.
[b]Reference 42.
[c]Reference 8.
[d]Reference 19.
[e]Reference 37.
[f]Reference 12.

Downloaded 21 Aug 2008 to 169.229.32.135. Redistribution subject to AIP license or copyright; see http://jcp.aip.org/jcp/copyright.jsp

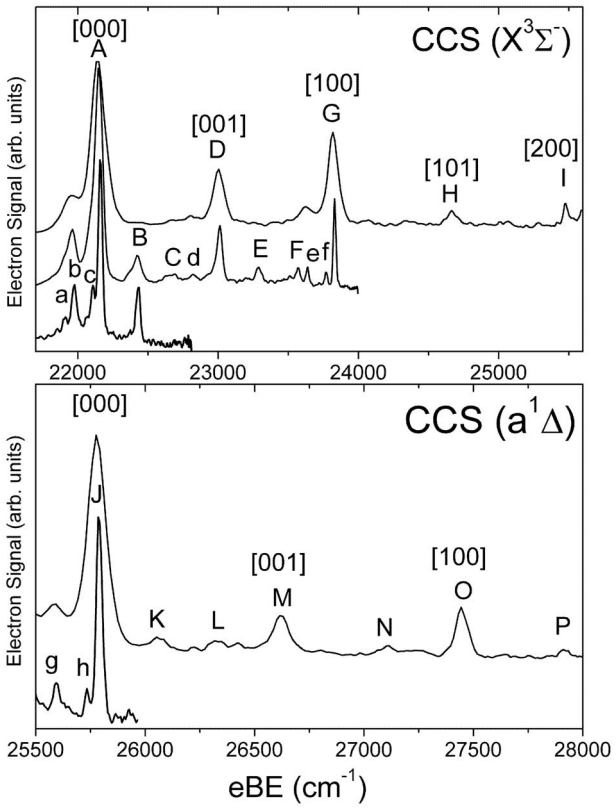

FIG. 3. SEVI spectra of CCS^- in the 21 500–28 000 cm^{-1} eBE range. The top panel displays traces taken at photon energies of 26 316, 24 213, and 22 989 cm^{-1}, while the lower panel displays traces taken at 29 369 and 26 316 cm^{-1}. The traces are vertically offset for clarity.

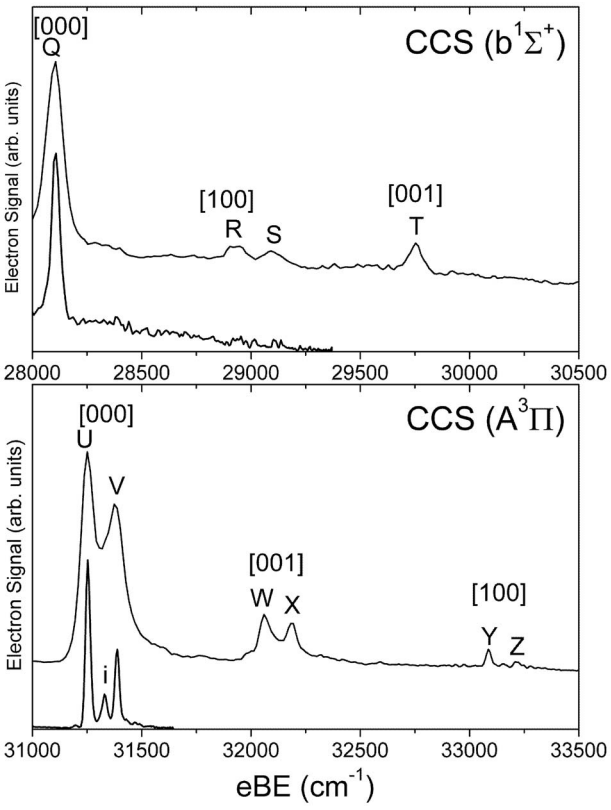

FIG. 4. SEVI spectra of CCS^- in the 28 000–30 500 cm^{-1} eBE range. The top panel displays traces taken at photon energies of 31 646 and 29 369 cm^{-1}, while the lower panel displays traces taken at 33 727 and 31 646 cm^{-1}. The traces are vertically offset for clarity.

peaks B and E, have a PAD indicative of $s+d$-wave detachment, while transitions associated with the $A\ ^3\Pi$ band have a p-wave character.

The SEVI spectra of CCS^- display more vibrational activity than the CCO^- spectra. In the top panel of Fig. 3, most of the transitions to the $X\ ^3\Sigma^-$ state can be assigned based on the previous observations by LIF (Ref. 30) and recent calculations by Tarroni *et al.*[9] Peaks B, D, and G are assigned to the 2_0^1, 3_0^1, and 1_0^1 transitions within the $X\ ^3\Sigma^-$ band, in agreement with the previous observations.[30] Peaks C and I are assigned to the 2_0^2 and 1_0^2 transitions, respectively. Peaks E and F are assigned to the $2_0^1 3_0^1$ and $2_0^2 3_0^1$ combination bands, while peak H is the $1_0^1 3_0^1$ combination band. Peaks B and E involve odd Δv transitions in the nontotally symmetric bending mode and are nominally forbidden. They have a p-wave PAD and their relative intensities increase when the detachment photon energy decreases. These points will be discussed in detail later.

Photodetachment transitions to the two singlet states of CCS are shown in the bottom panel of Fig. 3 and the top panel of Fig. 4. There is no experimental information reported for the vibrational levels of the $a\ ^1\Delta$ and $b\ ^1\Sigma^+$ states, but the observed vibrational progressions within these bands have very similar spacings to those of the $X\ ^3\Sigma^-$ band. The features are thus tentatively assigned to similar vibrational levels. Peaks K, M, and O in Fig. 3 are assigned to the 2_0^1, 3_0^1, and 1_0^1 fundamentals of the $a\ ^1\Delta$ state, respectively, yielding vibrational frequencies of 1660, 263, and 832 cm^{-1} for ν_1, ν_2, and ν_3. Using these values, the other transitions can be assigned to overtone and combination bands. Peak L is assigned to the 2_0^2 transition, while peaks N and P are assigned to the $2_0^2 3_0^1$ and $1_0^1 2_0^2$ combination bands, respectively. Photodetachment transitions to the $b\ ^1\Sigma^+$ state are displayed in the top panel of Fig. 4. Peaks R and T are assigned to the 3_0^1 and 1_0^1 transitions, yielding fundamental frequencies of 825 and 1645 cm^{-1} for these modes in the $b\ ^1\Sigma^+$ state. Peak S does not fit any vibrational levels on the $b\ ^1\Sigma^+$ state and is therefore assigned to the 1_0^2 transition of the $a\ ^1\Delta$ state.

Transitions to the $A\ ^3\Pi$ state are presented in the bottom panel of Fig. 4. Peaks U and V are separated by 133 cm^{-1} and are assigned to the $^3\Pi_2$ and $^3\Pi_1$ spin-orbit components of the $A\ ^3\Pi$ state origin transition. This splitting is in excellent agreement with calculations by Tarroni *et al.*[9] The $^3\Pi_0$ state is not observed because a photodetachment transition from a $^2\Pi_{3/2}$ anion state to a $^3\Pi_0$ neutral state requires a spin-flip which is nominally forbidden. The two remaining doublets are thus assigned to vibrations belonging to the same two spin-orbit states. Peaks W and X are assigned to the 3_0^1 fundamental, while peaks Y and Z are assigned to the 1_0^1 level. This is the first observation of the ν_3 mode in the $A\ ^3\Pi$ state of CCS. The $^3\Pi_2$ and $^3\Pi_1$ components of ν_3 are found to be 807 and 936 cm^{-1} above the $A\ ^3\Pi_2$ ground state, respectively. These values are slightly larger than the 788 and 913 cm^{-1} calculated by Tarroni *et al.*[9] The position of both ν_1 spin-orbit multiplets are in excellent agreement with the previous observations (see Table II).[29]

Downloaded 21 Aug 2008 to 169.229.32.135. Redistribution subject to AIP license or copyright; see http://jcp.aip.org/jcp/copyright.jsp

TABLE II. Peak positions, PAD, and assignments for the CCS^- SEVI spectra.

Peak	Position (cm^{-1})	Offset (cm^{-1})	PAD	Previous Obs[a] (cm^{-1})	Calculated[b] (cm^{-1})	Assignment (Vib)	Assignment (Electronic states)
a	21 910	−250	*s+d*			2_1^1	$X\,^3\Sigma^- \leftarrow X\,^2\Pi(\Sigma^-_{1/2},\Delta_{3/2})$
b	21 983	−195	*s+d*			0_0^0	$X\,^3\Sigma^- \leftarrow X\,^2\Pi_{1/2}$
c	22 108	−52	*s+d*			2_1^1	$X\,^3\Sigma^- \leftarrow X\,^2\Pi(\Sigma^+_{1/2},\Delta_{5/2})$
A	22 160	0	*s+d*			0_0^0	$X\,^3\Sigma^- \leftarrow X\,^2\Pi_{3/2}$
B	22 430	270	*p*	266.6	268	2_0^1	$X\,^3\Sigma^- \leftarrow X\,^2\Pi_{3/2}$
C	22 685	525	*s+d*	532.8	540	2_0^2	$X\,^3\Sigma^- \leftarrow X\,^2\Pi_{3/2}$
d	22 821	661	*s+d*			3_0^1	$X\,^3\Sigma^- \leftarrow X\,^2\Pi_{1/2}$
D	23 010	850	*s+d*	857.8	850	3_0^1	$X\,^3\Sigma^- \leftarrow X\,^2\Pi_{3/2}$
E	23 288	1128	*p*		1125	$2_0^1 3_0^1$	$X\,^3\Sigma^- \leftarrow X\,^2\Pi_{3/2}$
F	23 568	1408	*s+d*		1404	$2_0^2 3_0^1$	$X\,^3\Sigma^- \leftarrow X\,^2\Pi_{3/2}$
e	23 636	1476	*s+d*			1_0^1	$X\,^3\Sigma^- \leftarrow X\,^2\Pi_{1/2}$
f	23 770	1610	*s+d*			$1_0^1 2_1^1$	$X\,^3\Sigma^- \leftarrow X\,^2\Pi(\Sigma^+_{1/2},\Delta_{5/2})$
G	23 831	1671	*s+d*	1670.8	1661	1_0^1	$X\,^3\Sigma^- \leftarrow X\,^2\Pi_{3/2}$
H	24 668	2508	*s+d*	2511.6	2494	$1_0^1 3_0^1$	$X\,^3\Sigma^- \leftarrow X\,^2\Pi_{3/2}$
I	25 479	3319	*s+d*	3318.4	3298	1_0^2	$X\,^3\Sigma^- \leftarrow X\,^2\Pi_{3/2}$
g	25 595	−195	*s+d*			0_0^0	$a\,^1\Delta \leftarrow X\,^2\Pi_{1/2}$
h	25 735	−55	*s+d*			2_1^1	$a\,^1\Delta \leftarrow X\,^2\Pi(\Sigma^+_{1/2},\Delta_{5/2})$
J	25 790	0	*s+d*			0_0^0	$a\,^1\Delta \leftarrow X\,^2\Pi_{3/2}$
K	26 053	263				2_0^1	$a\,^1\Delta \leftarrow X\,^2\Pi_{3/2}$
L	26 320	530				2_0^2	$a\,^1\Delta \leftarrow X\,^2\Pi_{3/2}$
M	26 622	832	*s+d*		916[c]	3_0^1	$a\,^1\Delta \leftarrow X\,^2\Pi_{3/2}$
N	27 115	1325				$2_0^2 3_0^1$	$a\,^1\Delta \leftarrow X\,^2\Pi_{3/2}$
O	27 450	1660	*s+d*		1796[c]	1_0^1	$a\,^1\Delta \leftarrow X\,^2\Pi_{3/2}$
P	27 916	2126				$1_0^1 2_0^2$	$a\,^1\Delta \leftarrow X\,^2\Pi_{3/2}$
Q	28 106	0	*s+d*			0_0^0	$b\,^1\Sigma^+ \leftarrow X\,^2\Pi_{3/2}$
R	28 931	825	*s+d*			3_0^1	$b\,^1\Sigma^+ \leftarrow X\,^2\Pi_{3/2}$
S	29 091	3301	*s+d*			1_0^2	$a\,^1\Delta \leftarrow X\,^2\Pi_{3/2}$
T	29 751	1645	*s+d*			1_0^1	$b\,^1\Sigma^+ \leftarrow X\,^2\Pi_{3/2}$
U	31 254	0	*p*			0_0^0	$A\,^3\Pi_2 \leftarrow X\,^2\Pi_{3/2}$
i	31 330	76	*p*			0_0^0	$A\,^3\Pi_0 \leftarrow X\,^2\Pi_{1/2}$
V	31 387	133	*p*		133	0_0^0	$A\,^3\Pi_1 \leftarrow X\,^2\Pi_{3/2}$
W	32 061	807	*p*		788	3_0^1	$A\,^3\Pi_2 \leftarrow X\,^2\Pi_{3/2}$
X	32 190	936	*p*		913	3_0^1	$A\,^3\Pi_1 \leftarrow X\,^2\Pi_{3/2}$
Y	33 087	1833	*p*	1831[d]	1819	1_0^1	$A\,^3\Pi_2 \leftarrow X\,^2\Pi_{3/2}$
Z	33 217	1963	*p*	1962[d]	1957	1_0^1	$A\,^3\Pi_1 \leftarrow X\,^2\Pi_{3/2}$

[a]Reference 30 unless otherwise indicated.
[b]Reference 9 unless otherwise indicated.
[c]Reference 36.
[d]Reference 29.

There are many smaller peaks in Figs. 3 and 4 that appear to be from excited anion levels. Peaks b, e, and g each lie 195 cm^{-1} below a major transition. These peaks are assigned to hot bands originating from the excited spin-orbit state ($X\,^2\Pi_{1/2}$) of the anion. The resulting spin-orbit splitting is slightly larger than the value of −164 cm^{-1} calculated by Riaplov *et al.*[27] Peak i, in Fig. 4, is assigned to the 0_0^0 transition from the excited spin-orbit state of the anion to the neutral $A\,^3\Pi_0$ level. This transition does not require a spin-flip and is thus allowed. This assignment places the $^3\Pi_0$ level 271 cm^{-1} above the $^3\Pi_2$ level, approximately twice the splitting between the $^3\Pi_1$ and $^3\Pi_2$ levels, as expected.

The remaining small peaks are attributed to transitions from anion excited vibrational states. Because the main spectral features are 0-0 transitions and the most likely populated vibrational states are the low-frequency ν_2 bending modes, these peaks are assigned to sequence bands from bend-excited levels with $\Delta\nu_2=0$. The resulting energy level pattern is governed by Renner–Teller coupling in the $X\,^2\Pi$ state of CCS^-. The combination of spin-orbit and Renner–Teller coupling splits the degenerate $\nu_2=1$ state into four levels labeled $\Sigma^+_{1/2}$, $\Delta_{5/2}$, $\Delta_{3/2}$, and $\Sigma^+_{1/2}$. Panten *et al.*[41] calculated these levels to lie 310, 318, 480, and 492 cm^{-1} above the $X\,^2\Pi_{3/2}$ anion ground level, respectively. Using the experimental frequency of ν_2 in the neutral $X\,^3\Sigma^-$ state, the $\Delta\nu_2=0$ sequence bands starting from the anion $\nu_2=1$ levels should have binding energies of −43, −51, −213, and −225 cm^{-1} with respect to transitions originating from the anion $\nu_2=0$ level. Peak c at −52 cm^{-1} is thus assigned to a sequence band with $\Delta\nu=0$ transition starting from the $\Sigma^+_{1/2}$ and $\Delta_{5/2}$ anion $\nu_2=1$ components, while peak a at −250 cm^{-1} originates from the $\Delta_{3/2}$ and $\Sigma^+_{1/2}$ components. Because of the low intensity and small splitting of these transitions, the individual Σ and Δ components could not be resolved in our spectra. Peaks f and h are assigned to a sequence bands from the $\Sigma^+_{1/2}/\Delta_{5/2}$ anion $\nu_2=1$ states to the [100] level of the $X\,^3\Sigma^-$ state and the [000] level of the $a\,^1\Delta$ state, respectively.

Downloaded 21 Aug 2008 to 169.229.32.135. Redistribution subject to AIP license or copyright; see http://jcp.aip.org/jcp/copyright.jsp

TABLE III. Experimental and calculated values of the EAs and term energies of the four lowest-lying electronic states of CCO and CCS.

State	Current expt. $T_0 \pm 0.0006$ (eV)	Previous expt. T_0 (eV)	Calculated T_0 (eV)
CCO ($X\,^3\Sigma^-$)	0.0	0.0	0.0
($a\,^1\Delta$)	0.6539	0.653 ± 0.012[a]	0.63[b]
($b\,^1\Sigma^+$)	1.0170	1.024 ± 0.012[a]	1.00[b]
($A\,^3\Pi$)	1.4408	$1.440\,1788 \pm 0.000\,000\,1$[c]	1.34[b]
EA (CCO)	2.3107	2.310 ± 0.012[a]	2.22[b]
CCS ($X\,^3\Sigma^-$)	0.0	0.0	0.0
($a\,^1\Delta$)	0.4501	⋯	0.53[d]
($b\,^1\Sigma^+$)	0.7372	⋯	0.77[d]
($A\,^3\Pi$)	1.1275	1.1339 ± 0.002[e]	1.04[d]
EA(CCS)	2.7475	⋯	2.68[d]

[a]Reference 42.
[b]Reference 37.
[c]Reference 17.
[d]Reference 38.
[e]Reference 27.

IV. ANALYSIS AND DISCUSSION

This study determines precise EAs of CCO and CCS. The value of EA(CCO) is found to be 2.3107 ± 0.0006 eV, which lies within the uncertainty of the previous experimental value (2.310 ± 0.012) determined by PE spectroscopy.[42] The EA of CCS is 2.7475 ± 0.0006 eV; this is the first reported experimental value for EA(CCS). These values for the EA are slightly larger than those predicted by calculations. Zengin *et al.*[37] calculated an EA of 2.22 eV for CCO, while Riaplov *et al.*[27] predicted an EA of 2.68 eV for CCS.

The term energies of the four lowest electronic states of CCO and CCS determined in this study are listed in Table III. For CCO, the singlet term energies are consistent with those previously determined by PE spectroscopy[42] but are more precise. The first two singlet states, $a\,^1\Delta$ and $b\,^1\Sigma^+$, are 0.6539 ± 0.0006 and 1.0170 ± 0.0006 eV above the ground state, respectively, while the first excited triplet state lies 1.4408 ± 0.0006 eV above the ground state. The term energy for the $A\,^3\Pi$ state of CCO found here agrees with the previous observations from high-resolution absorption spectroscopy.[16,17] For the CCS radical, this study provides the first observation of the two low-lying singlet states. The $a\,^1\Delta$ and $b\,^1\Sigma^+$ states lie 0.4501 ± 0.0006 and 0.7372 ± 0.0006 eV above the ground state. These values are in good agreement with recent calculations by Zhang *et al.*,[38] which predicted term energies of 0.53 and 0.77 eV for the two first singlet states. Finally, the $A\,^3\Pi$ state is found to lie 1.1275 ± 0.0006 eV above the ground state, in accord with previous observations and calculations.[27,29]

The features in the SEVI spectra also comprise unresolved rotational structure. We found that modeling the rotational contours using *s*-wave detachment selection rules[53] yielded corrections smaller than 2 cm^{-1} to the EAs and term energies reported here. This insignificant correction reflects the very similar anion and neutral geometries, a situation that places the peak center very close to the band origin for each vibronic transition. An anion rotational temperature of 75 K was assumed in order to reproduce the ~20 cm^{-1} peak width observed at detachment close to threshold.

The numerous resolved vibrational transitions in the spectra of CCO and CCS allow us to probe the vibronic structure of these radicals. For example, in CCO and CCS, Herzberg–Teller vibronic coupling between the nearby $X\,^3\Sigma^-$ ground state and $A\,^3\Pi$ state can be detected by forbidden transitions in the bending mode. The SEVI spectrum of CCO^- displays vibrational activity only in the ν_1 and ν_3 modes for the four electronic states probed in this study. This is what is expected for a transition between two linear states with $C_{\infty v}$ symmetry since both modes are totally symmetric. It is also in excellent agreement with FC simulations based on the *ab initio* geometry and force constants of the anion and the uncoupled neutral states.[37] Carter *et al.*[8] recently calculated the spin-rovibronic levels of the $X\,^3\Sigma^-$ and $A\,^3\Pi$ states of CCO but neglected the vibronic coupling between the two states. Nonetheless, the calculated vibrational frequencies agree well with the experimental values measured here and in previous studies. This points out toward very weak vibronic interactions in the low-lying states of CCO.

However, the situation is different in the CCS^- SEVI spectrum, which exhibits considerably more vibrational activity, in general. All four bands show progressions in the ν_3 mode, whereas no activity in this mode was seen in the CCO^- SEVI spectra. Also, peaks B and E, which are assigned to the 2_0^1 and $2_0^1 3_0^1$ transitions, involve odd $\Delta\nu$ transitions of nontotally symmetric modes and are thus nominally forbidden in PE spectroscopy. It is thus useful to simulate the spectrum within the FC approximation to determine whether differences with CCO^- arise from simple geometric effects or from vibronic coupling, Duschinsky rotation, or other effects that can arise in PE spectroscopy. We note that FC simulations were carried out by Panten *et al.*[41] using calculated geometries and force constants for the anion and neutral ground states but these simulations predict more activity in the ν_3 mode than the ν_1 mode. This result is not consistent with the experimental spectrum, in which the ν_1 mode is more active.

We have performed two sets of FC simulations using the parallel mode approximation that are shown in Fig. 5 along with the experimental spectra. For the first simulation, shown in the middle panel of Fig. 5, we used the geometries and frequencies calculated by Panten *et al.*[41] for both the anion and neutral. This simulation yielded a PES spectrum that overestimates the ν_3 activity and underestimates the ν_1 activity. In the second simulation, shown in the bottom panel of Fig. 5, we use the known experimental geometry[25] ($R_{CC}=1.2771$ Å and $R_{CS}=1.6477$ Å) and vibrational frequencies[30] of the $X\,^3\Sigma^-$ neutral state and the anion bond length was adjusted to fit the experimental spectra. The best fit was obtained with a CC bond length of 1.268 Å and a CS bond length of 1.646 Å. These values are close to the bond lengths calculated by Panten *et al.*[41] The fact that the intensities of the ν_1 and ν_3 features could be reproduced with a reasonable anion geometry is consistent with the calculations of Tarroni *et al.*,[9] which found mixing of only 2%–3% for the ν_1 and ν_3 modes. Moreover, the vibrational frequencies calculated by Tarroni *et al.*[9] for these two modes agree well with those found in this study.

The only features not accounted for by the FC simula-

Downloaded 21 Aug 2008 to 169.229.32.135. Redistribution subject to AIP license or copyright; see http://jcp.aip.org/jcp/copyright.jsp

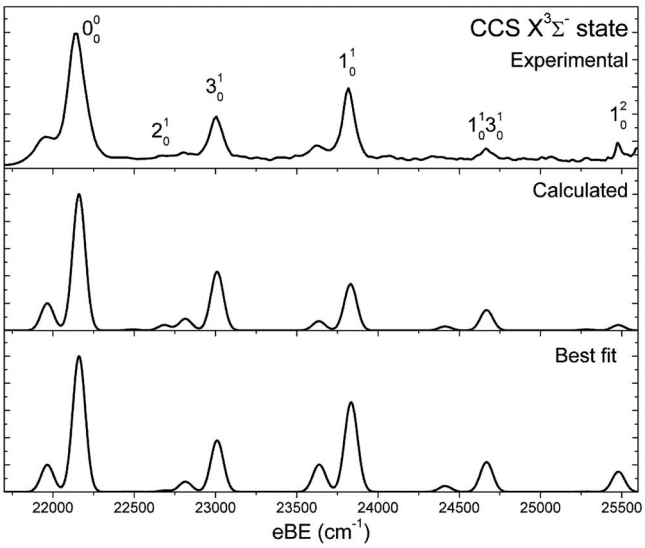

FIG. 5. FC simulation of the CCS $X\,^3\Sigma^-$ state photodetachment spectrum. The top panel displays the SEVI spectrum taken at photon energy of 26 316 cm^{-1}. The middle panel shows the simulated spectrum using the geometries and frequencies calculated by Panten *et al.* (Ref. 41). The lower panel displays the best fit obtained by optimizing the anion geometry. (See text for details.)

tion are the two peaks involving odd quanta of bending excitation. These two nominally forbidden peaks have a different PAD than the other $X\,^3\Sigma^-$ features, which is reminiscent of the C_2H^- SEVI spectrum.[52] The *p*-wave character of these features is a clear indication that these features are gaining intensity from vibronic coupling between the $X\,^3\Sigma^-$ and $A\,^3\Pi$ states induced by the bending mode. The *p* PADs of peaks B and E also explain why the relative intensities is larger at lower photodetachment energies. According to the Wigner threshold law,[51] the photodetachment cross section (σ) near threshold is given by

$$\sigma \propto (\Delta E)^{l+1/2}, \tag{2}$$

where ΔE is the difference between the energy of the photon and the detachment threshold and l is the angular momentum of the ejected electron. In the energy range presented in Fig. 3, the *d* component ($l=2$) cross section of the ($s+d$)-wave drops faster than the cross section for a *p*-wave ($l=1$) detachment when the photon energy is lowered. This leads to increased intensities of peaks B and E relative to the other transitions as the photodetachment energy is lowered. Note that this trend in the relative intensities is opposite to what was observed in the C_2H^- SEVI spectrum because the allowed transitions were almost pure *s*-wave with very small *d*-wave contribution.[52]

V. CONCLUSIONS

The high-resolution PE spectra of CCO and CCS using the SEVI technique are reported. This work provides precise EAs as well as term energies of the neutral $X\,^3\Sigma^-$, $a\,^1\Delta$, $b\,^1\Sigma^+$, and $A\,^3\Pi$ electronic states of these two species. Several previously unobserved vibronic transitions on these four states are resolved. The CCS spectrum reveals evidence of small vibronic coupling between the electronic states. The analysis of hot bands allowed the first experimental observation of the spin-orbit orbit splitting on the $X\,^2\Pi$ ground state of CCO and CCS.

ACKNOWLEDGMENTS

This work was supported by the Air Force Office of Scientific Research under Grant No. F49620-03-1-0085. E.G. thanks the National Science and Engineering Research Council of Canada (NSERC) for a post graduate scholarship and T.Y. thanks the Fonds Québécois de la Recherche sur la Nature et les Technologies (FQRNT) for a masters scholarship.

[1] M. Ohishi, H. Suzuki, S. I. Ishikawa, C. Yamada, H. Kanamori, W. M. Irvine, R. D. Brown, P. D. Godfrey, and N. Kaifu, Astrophys. J. **380**, L39 (1991).
[2] S. Saito, K. Kawaguchi, S. Yamamoto, M. Ohishi, H. Suzuki, and N. Kaifu, Astrophys. J. **317**, L115 (1987).
[3] K. D. Bayes, J. Chem. Phys. **52**, 1093 (1970).
[4] K. H. Becker and K. D. Bayes, J. Chem. Phys. **48**, 653 (1968).
[5] A. Fontijn and S. E. Johnson, J. Chem. Phys. **59**, 6193 (1973).
[6] I. dc Gregorio-Monsalvo, J. F. Gomez, O. Suarez, T. B. H. Kuiper, L. F. Rodriguez, and E. Jimenez-Bailon, Astrophys. J. **642**, 319 (2006).
[7] W. D. Langer, T. Velusamy, T. B. H. Kuiper, S. Levin, E. Olsen, and V. Migenes, Astrophys. J. **453**, 293 (1995).
[8] S. Carter, N. C. Handy, and R. Tarroni, Mol. Phys. **103**, 1131 (2005).
[9] R. Tarroni, S. Carter, and N. C. Handy, Mol. Phys. **105**, 1129 (2007).
[10] Y. Ohshima, Y. Endo, and T. Ogata, J. Chem. Phys. **102**, 1493 (1995).
[11] C. Yamada, S. Saito, H. Kanamori, and E. Hirota, Astrophys. J. **290**, L65 (1985).
[12] H. Abe, Y. Kawamoto, M. Fujitake, N. Ohashi, T. Momose, and T. Shida, J. Mol. Spectrosc. **180**, 277 (1996).
[13] H. Abe, T. Kikuchi, K. Takahashi, M. Fujitake, and N. Ohashi, J. Mol. Spectrosc. **167**, 353 (1994).
[14] H. Abe, M. Mukai, M. Fujitake, and N. Ohashi, J. Mol. Spectrosc. **195**, 317 (1999).
[15] Z. Abusara, T. S. Sorensen, and N. Moazzen-Ahmadi, J. Chem. Phys. **119**, 9491 (2003).
[16] C. Devillers and D. A. Ramsay, Can. J. Phys. **49**, 2839 (1971).
[17] M. Fujitake, R. Kiryu, and N. Ohashi, J. Mol. Spectrosc. **154**, 169 (1992).
[18] M. E. Jacox, D. E. Milligan, N. G. Moll, and W. E. Thompson, J. Chem. Phys. **43**, 3734 (1965).
[19] N. Moazzen-Ahmadi and R. T. Boere, J. Chem. Phys. **110**, 955 (1999).
[20] N. Moazzen-Ahmadi, D. W. D. Sandilands, and R. T. Boere, Chem. Phys. Lett. **265**, 563 (1997).
[21] N. Ohashi, R. Kiryu, S. Okino, and M. Fujitake, J. Mol. Spectrosc. **157**, 50 (1993).
[22] C. Yamada, H. Kanamori, H. Horiguchi, S. Tsuchiya, and E. Hirota, J. Chem. Phys. **84**, 2573 (1986).
[23] W. M. Pitts, V. M. Donnelley, A. P. Baronavski, and J. R. McDonald, Chem. Phys. **61**, 451 (1981).
[24] M. Ikeda, Y. Sekimoto, and S. Yamamoto, J. Mol. Spectrosc. **185**, 21 (1997).
[25] S. Yamamoto, S. Saito, K. Kawaguchi, Y. Chikada, H. Suzuki, N. Kaifu, S. Ishikawa, and M. Ohishi, Astrophys. J. **361**, 318 (1990).
[26] G. Maier, H. P. Reisenauer, and R. Ruppel, Eur. J. Org. Chem. **2004**, 4197 (2004).
[27] E. Riaplov, M. Wyss, J. P. Maier, D. Panten, G. Chambaud, P. Rosmus, and J. Fabian, J. Mol. Spectrosc. **222**, 15 (2003).
[28] H. Y. Wang, J. Szczepanski, A. Cooke, P. Brucat, and M. Vala, Int. J. Quantum Chem. **102**, 806 (2005).
[29] M. Nakajima, Y. Sumiyoshi, and Y. Endo, J. Chem. Phys. **117**, 9327 (2002).
[30] A. J. Schoeffler, H. Kohguchi, K. Hoshina, Y. Ohshima, and Y. Endo, J. Chem. Phys. **114**, 6142 (2001).
[31] D. Begue, P. Carbonniere, and C. Pouchan, J. Phys. Chem. A **105**, 11379 (2001).

Downloaded 21 Aug 2008 to 169.229.32.135. Redistribution subject to AIP license or copyright; see http://jcp.aip.org/jcp/copyright.jsp

[32] S. T. Brown, Y. Yamaguchi, and H. F. Schaefer, J. Phys. Chem. A **104**, 3603 (2000).
[33] S. Mishra, W. Domcke, and L. V. Poluyanov, Chem. Phys. Lett. **446**, 256 (2007).
[34] I. Perez-Juste, A. M. Grana, L. Carballeira, and R. A. Mosquera, J. Chem. Phys. **121**, 10447 (2004).
[35] Y. M. Xie and H. F. Schaefer, J. Chem. Phys. **96**, 3714 (1992).
[36] Z. L. Cai, X. G. Zhang, and X. Y. Wang, Chem. Phys. Lett. **213**, 168 (1993).
[37] V. Zengin, B. J. Persson, K. M. Strong, and R. E. Continetti, J. Chem. Phys. **105**, 9740 (1996).
[38] J. L. Zhang, W. P. Wu, L. B. Wang, and Z. X. Cao, J. Chem. Phys. **124**, 124319 (2006).
[39] J. Fulara, M. Grutter, M. Wyss, and J. P. Maier, J. Phys. Chem. A **102**, 3459 (1998).
[40] D. Panten, G. Chambaud, P. Rosmus, and P. J. Knowles, Chem. Phys. Lett. **311**, 390 (1999).
[41] D. Panten, G. Chambaud, P. Rosmus, E. Riaplov, and J. P. Maier, Z. Phys. Chem. **217**, 231 (2003).
[42] H. Choi, D. H. Mordaunt, R. T. Bise, T. R. Taylor, and D. M. Neumark, J. Chem. Phys. **108**, 4070 (1998).
[43] J. M. Oakes, M. E. Jones, V. M. Bierbaum, and G. B. Ellison, J. Phys. Chem. **87**, 4810 (1983).
[44] M. J. Nee, A. Osterwalder, J. Zhou, and D. M. Neumark, J. Chem. Phys. **125**, 014306 (2006).
[45] A. Osterwalder, M. J. Nee, J. Zhou, and D. M. Neumark, J. Chem. Phys. **121**, 6317 (2004).
[46] A. Eppink and D. H. Parker, Rev. Sci. Instrum. **68**, 3477 (1997).
[47] U. Even, J. Jortner, D. Noy, N. Lavie, and C. Cossart-Magos, J. Chem. Phys. **112**, 8068 (2000).
[48] W. C. Wiley and I. H. McLaren, Rev. Sci. Instrum. **26**, 1150 (1955).
[49] D. W. Chandler and P. L. Houston, J. Chem. Phys. **87**, 1445 (1987).
[50] J. Cooper and R. N. Zare, J. Chem. Phys. **48**, 942 (1968).
[51] E. P. Wigner, Phys. Rev. **73**, 1002 (1948).
[52] J. Zhou, E. Garand, and D. M. Neumark, J. Chem. Phys. **127**, 114313 (2007).
[53] Y. X. Zhao, I. Yourshaw, G. Reiser, C. C. Arnold, and D. M. Neumark, J. Chem. Phys. **101**, 6538 (1994).

Downloaded 21 Aug 2008 to 169.229.32.135. Redistribution subject to AIP license or copyright; see http://jcp.aip.org/jcp/copyright.jsp